

## EVOLUTION AND NUCLEOSYNTHESIS OF METAL-FREE MASSIVE STARS

HIDEYUKI UMEDA, KEN'ICHI NOMOTO, TAKAYOSHI NAKAMURA

Department of Astronomy, and Research Center for the Early Universe, School of Science, University of Tokyo,  
Bunkyo-ku, Tokyo 113-0033, Japan

E-mail: umeda@astron.s.u-tokyo.ac.jp; nomoto@astron.s.u-tokyo.ac.jp; nakamura@astron.s.u-tokyo.ac.jp

### ABSTRACT

We calculate presupernova evolutions and supernova explosions of massive stars ( $M = 13 - 25M_{\odot}$ ) for various metallicities. We find the following characteristic abundance patterns of nucleosynthesis in the metal-free (Pop III) stars. (1) The  $\alpha$ -nuclei (from C to Zn) are more efficiently produced than other isotopes, and the abundance pattern of  $\alpha$ -nuclei can be similar to the solar abundance. In particular, near solar ratios of alpha elements/Fe might be a signature of Pop III which could produce a large amount of Fe. (2) The abundance ratios of odd  $Z$  to even  $Z$  elements such as Na/Mg and Al/Mg become smaller for lower metallicity. However, these ratios almost saturate below  $Z \lesssim 10^{-5}$ , and  $[\text{Na}, \text{Al}/\text{Mg}] \sim -1$  for Pop III and low metal Pop II nucleosynthesis. This result is consistent with abundance pattern of metal poor stars, in which these ratios also saturate around  $-1$ . We suggest that these stars with the lowest  $[\text{Na}/\text{Mg}]$  or  $[\text{Al}/\text{Mg}]$  may contain the abundance pattern of Pop III nucleosynthesis. (3) Metal poor stars show interesting trends in the ratios of  $[\text{Cr}, \text{Mn}, \text{Co}/\text{Fe}]$ . We discuss that these trends are not explained by the differences in metallicity, but by the relative thickness between the complete and the incomplete Si burning layers. Large  $[\text{Co}/\text{Fe}]$  and small  $[\text{Cr}, \text{Mn}/\text{Fe}]$  values found in the observations are explained if mass cut is deep or if matter is ejected from complete Si burning layer in a form of a jet or bullets. (4) We also find that primary  $^{14}\text{N}$  production occurs in the massive Pop III stars, because these stars have radiative H-rich envelopes so that the convective layer in the He-shell burning region can reach the H-rich region.

### 1. INTRODUCTION

Very metal poor stars provide important clues to investigate early cosmic and galactic chemical evolution because their abundance patterns would tell us what kind of stars (including the First Stars) contribute to form those patterns. We might be able to identify the signature of the First Stars and thus can learn how the universe and galaxies evolved chemically in its early phase. Such identification would be possible in the abundance pattern of an individual metal-poor star, because in early phase of the galaxy evolution the ejecta of each supernova may not have enough time to be uniformly mixed in the galaxy (Audouze & Silk 1995; Ryan et al. 1996; Shigeyama & Tsujimoto 1998).

One example is the interesting trends of  $[\text{Cr}/\text{Fe}]$ ,  $[\text{Mn}/\text{Fe}]$  and  $[\text{Co}/\text{Fe}]$  with  $[\text{Fe}/\text{H}]$  (McWilliam et al. 1995ab; Ryan et al. 1996; McWilliam 1997). Since the published SNe II yields (Woosley & Weaver 1995, hereafter WW95; Thielemann, Nomoto & Hashimoto 1996; Hashimoto 1995; Tsujimoto et al. 1995; Nomoto et al. 1997) are not consistent with these trends, one might suspect that these trends would be a signature of Pop III star yields.

Here we define the First Stars as metal-free (Pop III) stars. We evolve and explode massive metal-free stars as well as other metallicity stars including the metallicity dependent mass loss. We calculate nucleosynthesis to see what are the indications of the ejecta of the first stars. Previously, WW95, Arnett (1996), and Limongi et al. (1999, LCS) calculated nucleosynthesis of SNe II using for various metallicities down to metal-free, but these studies did not include mass loss and did not examine the dependence on the convective mixing.

In addition to the metallicity effects, we study the dependence on the explosion energy. This is because some recent supernovae have been recognized to be hyper-energetic (hypernovae) being more than  $10^{52}$  ergs. The examples include SN 1998bw (Galama et al. 1998; Iwamoto et al. 1998; Woosley et al. 1999), SN 1997ef (Iwamoto et al. 1999), and SN 1997cy (Germany et al. 1999; Turatto et al. 1999). These hypernovae are suggested to originate from quite massive stars, so that their nucleosynthesis may significantly contribute to the early cosmic and galactic chemical evolution.

Our results are also sensitive to the efficiency of convective mixing. Here we report mostly the case of low efficiency, and more complete results will be presented in a forthcoming paper.

### 2. CODE AND METHOD

We have developed a stellar evolution code which is based on Henyey type stellar evolution codes by Nomoto & Hashimoto (1988, NH88), Saio & Nomoto (2000), and Umeda et al. (1999). We start calculations from the zero-age main-sequence through core collapse including metallicity dependent mass loss (de Jager et al. 1988; Kudritzki et al. 1989). For example, the star of initially  $25 M_{\odot}$  with solar metallicity decreases its mass down to  $21.5 M_{\odot}$  before the explosion.

We adopt the OPAL opacity as a function of metallicity,  $X(\text{H})$ ,  $X(\text{C})$  and  $X(\text{O})$  (Iglesius & Rodgers 1993). This code runs a nuclear reaction network by Hix & Thielemann (1996) for the calculation of nuclear energy generation and nucleosynthesis. For nucleosynthesis of H and He burning, 51 isotopes up to Si are included, and after He burning 240 isotopes up to Ge are included.

Schwartzschild criterion is adopted for convective stability criterion and diffusive convective mixing by Spruit (1992) is adopted. In this work, a case for relatively slow mixing,  $f_k = 0.05$  (Saio & Nomoto 2000), is investigated.

At the end of core helium burning, the central C/O ratio is largely influenced by the uncertain  $^{12}\text{C}(\alpha, \gamma)^{16}\text{O}$  reaction rate (Fowler 1984). The C/O ratio affects the abundances of Ne, Mg and Al, and also the Fe core mass.

In this work, the  $^{12}\text{C}(\alpha, \gamma)^{16}\text{O}$  reaction rate is chosen to be 1.4 times the value given in Caughlan & Fowler (1988; CF88). With this choice for the  $25 M_\odot$  model of  $Z=0.02$ , the central C/O ratio is 0.2 at the end of core helium burning, which is close to the NH88 models.

Using the presupernova models, we carry out 1D hydrodynamical simulations of SN II explosions with a PPM code which uses a small nuclear reaction network. Then the explosive nucleosynthesis is calculated as a post-processing using a larger reaction network of 300 isotopes up to Br as described in Thielemann et al. (1996).

### 3. PRESUPERNOVA STELLAR EVOLUTION

Figure 1 shows the H-R diagram of the  $25 M_\odot$  star with metallicity of  $Z = 0, 0.001, \text{ and } 0.02$ . As shown in this figure, the star is more luminous for lower metallicity owing to the smaller opacity. The evolution in the H-R diagram of zero metal (Pop III) stars with  $13 M_\odot \lesssim M \lesssim 25 M_\odot$  are quite different from Pop I and II stars, because they do not evolve to red-giants before core collapse (e.g., Castellani et al. 1983).

Figures 2 shows abundance distribution of presupernova stars. The H-rich envelope for  $Z = 0.02$  is convective, while the H-rich envelope for  $Z = 0$  is radiative. For  $Z = 0$ , only a small amount of CNO elements are produced in the H-rich layer, so that hydrogen burning is too weak to drive the expansion toward a red-giant.

For Pop I and II stars, lower metallicity leads to the formation of a more massive core because of the larger luminosity. One might expect Pop III stars have the largest cores because of this effect; however, the He core size is smaller than Pop II because of weak H-shell burning. In our model these two effects cancel out and the masses of the He and C-O cores are almost the same between  $Z = 0$  and  $Z = 0.02$  models (Fig. 2).

#### 3.1. Fe Core Mass

The Fe core mass is mostly determined by the He (or C-O) core mass, and the C/O ratio after the central helium burning. In general, a larger He (or C-O) core mass leads to a larger Fe core mass. The larger C/O ratio leads to weaker central O-burning and a smaller Fe core mass.

A more massive or lower (but non-zero) metallicity star tends to have a larger luminosity and hence a larger He (and C-O) core mass. Also the C/O ratio is smaller for a larger core mass. Therefore, the Fe core mass tends to be larger for a larger stellar mass and smaller metallicity, although its size also depends on the behavior of convection and these relations do not hold always.

Figure 3 summarizes the masses of the presupernova Fe cores compared with other works. We should note that all other works did not include mass loss.

Although opacity is smaller, Pop III stars have smaller core masses than Pop II stars for the same main-sequence

mass because H-burning via the CNO cycle is weaker. Since the Pop II stars have larger cores than Pop I, the core masses of Pop III are closer to Pop I rather than Pop II. Note that this relation does not always hold since the core mass depends on the behavior of convection which is rather chaotic (Barkat et al. 1990).

#### 3.2. $Y_e$ distribution

The electron mole number  $Y_e$  is important for the explosive nucleosynthesis. In Figure 4 we show the distribution of  $Y_e$  in the presupernova model. This shows that  $Y_e$  is larger for zero metal stars than solar metallicity stars, because of smaller  $^{22}\text{Ne}$  which is produced from  $^{14}\text{N}$ .

## 4. EXPLOSIVE NUCLEOSYNTHESIS

The general features of the explosive nucleosynthesis in SNe II are summarized as follows (e.g., Woosley et al. 1973; Hashimoto et al. 1989; Thielemann et al. 1994, 1996). The explosively produced elements depend mainly on the peak temperature attained through the passage of the shock. The region after the shock passage is radiation dominant, so that the peak temperature is approximately related to the stellar radius  $r$  and the deposited energy  $E^*$  as

$$T_9 = (E_{51}^*)^{1/4} (r/3.16 \times 10^4 \text{ km})^{-3/4}, \quad (1)$$

where  $E_{51}^*$  is the deposited energy in units of  $10^{51}$  erg,  $T_9$  is the peak temperature in  $10^9$  K. Therefore, assuming  $E_{51}^* = 1$ , explosive nuclear burning are classified into several cases according to  $T_9$  (or  $r$ ) at  $T_9 = 5$  ( $r = 3700$  km),  $T_9 = 4$  ( $r = 4980$  km),  $T_9 = 3.3$  ( $r = 6430$  km), and  $T_9 = 2.1$  ( $r = 11,800$  km). The relation between the presupernova radius  $r$  and the enclosed mass  $M_r$  depends on the progenitor's mass and metallicity (e.g., Nomoto et al. 1993).

#### 4.1. Complete Silicon Burning and Neutron-rich Species

For  $T_9 > 5$ , explosive silicon and oxygen burning leads to nuclear statistical equilibrium and produces mostly  $^{56}\text{Ni}$  if  $Y_e > 0.49$ ,  $T_9 < 8$ , and  $\rho < 10^8 \text{ g cm}^{-3}$ . Other iron peak elements are also produced owing to this high temperature but the final products depend on the time scale of the freezeout and initial distribution of  $Y_e$ .

For the inner region,  $\alpha$ -rich freeze out occurs after complete silicon burning. Some  $^4\text{He}$  remain even after the freezeout without recombining into the iron peak elements. In these regions, appreciable amount of radioactive nuclei,  $^{56}\text{Ni}$ ,  $^{57}\text{Ni}$ , and  $^{44}\text{Ti}$ , are produced. Also  $^{56,57}\text{Fe}$  and  $^{58,60,62}\text{Ni}$  are synthesized here.  $^{60,62}\text{Ni}$  are originally produced as  $^{60,62}\text{Zn}$  which decay as  $^{60,62}\text{Zn} \rightarrow ^{60,62}\text{Cu} \rightarrow ^{60,62}\text{Ni}$ . These neutron-rich nuclei ( $Y_e = 0.484$  for  $^{62}\text{Zn}$  and  $Y_e = 0.483$  for  $^{58}\text{Ni}$ ) are produced in the neutron-rich layers near the mass cut in SNe II as well as in Type Ia supernovae.

In smaller mass stars, a larger amount of neutron-rich elements  $^{58}\text{Ni}$ ,  $^{60,62}\text{Zn}$  are produced near the mass cut. The mass cut is related to the amount of radioactive nuclei. The most important ones are  $^{56}\text{Ni}$  and  $^{57}\text{Co}$  ( $^{57}\text{Ni} \rightarrow ^{57}\text{Co} \rightarrow ^{57}\text{Fe}$ ) as actually observed in SN 1987A

(e.g., Arnett et al. 1989; Nomoto et al. 1994) and the obtained ratio  $^{56}\text{Ni}/^{57}\text{Ni}$  was used to infer the mass cut (Kumagai et al. 1989, 1993).

#### 4.2. Incomplete Silicon Burning and Explosive Oxygen Burning

For  $4 < T_9 < 5$ , incomplete silicon burning and explosive oxygen burning produce mostly  $^{28}\text{Si}$ ,  $^{32}\text{S}$ ,  $^{36}\text{Ar}$  and  $^{40}\text{Ca}$ . Some  $^{44}\text{Ti}$  and  $^{56}\text{Ni}$  are also produced by incomplete silicon burning. Oxygen is burned up completely and  $^{28}\text{Si}$ ,  $^{32}\text{S}$  and other  $\alpha$ -particle nuclei are produced. The peak temperature is too low to produce iron peak elements.

For  $3.3 < T_9 < 4.0$ , explosive neon burning produces some amounts of  $^{16}\text{O}$ ,  $^{28}\text{Si}$ , and  $^{32}\text{S}$ .

For  $2.0 < T_9 < 3.3$ , explosive carbon burning produces  $^{20}\text{Ne}$ ,  $^{24}\text{Mg}$ . However, the peak temperature is too low to change the initial abundances appreciably. For  $T_9 < 2$ , no significant explosive burning occurs. For the oxygen-rich layer with  $2 < T_9 < 3$ , where explosive neon and carbon burning take place, the p-process occurs via the photodisintegration of nuclei:  $(\gamma, p)$ ,  $(\gamma, n)$ ,  $(\gamma, \alpha)$  (e.g., Rayet et al. 1995).

The inner part of the star where  $T_9 > 2$  undergoes the explosive nucleosynthesis according to the above classification. The outer part, including most of the original oxygen-rich layer, is ejected without being processed by explosive nuclear burning. The ratio between the explosive and hydrostatic burning products is sensitive to the stellar mass.

### 5. ABUNDANCE DISTRIBUTION

Figures 5–8 show the abundance distribution of some isotopes before and  $10^3$  sec after explosive nuclear burning for the  $20 M_\odot$  star with  $Z = 0$  and  $0.02$ . These figures show that  $Z = 0$  and  $0.02$  models yield roughly the same amount of alpha nuclei which are produced during He and C-burnings such as  $^{12}\text{C}$ ,  $^{16}\text{O}$ ,  $^{20}\text{Ne}$ ,  $^{24}\text{Mg}$ , and produced during explosive burning such as  $^{40}\text{Ca}$ ,  $^{44}\text{Ti}$ ,  $^{52}\text{Fe}$ ,  $^{64}\text{Ge}$ . On the other hand, other elements produced during H, He and C-burnings such as  $^{13}\text{C}$ ,  $^{14}\text{N}$ ,  $^{15}\text{N}$ ,  $^{23}\text{Na}$ ,  $^{27}\text{Al}$ ,  $^{31}\text{P}$  are much less abundant in the  $Z = 0$  model compared with the  $Z = 0.02$  model. This also can be seen in Figure 11.

As examples of these two types of species, we discuss the ejected masses of radioactive species  $^{26}\text{Al}$  and  $^{44}\text{Ti}$  (decays into  $^{44}\text{Ca}$ ), which are important for the Line Gamma-Ray astronomy. The  $^{44}\text{Ti}$  mass is in general roughly independent of metallicity, but depends sensitively on the mass cut. In Figure 11,  $^{44}\text{Ti}$  and all heavy elements with  $A \geq 60$  appear to be much less abundant for  $Z = 0$  than  $Z = 0.02$ . This is only because the mass cut is set to produce  $0.07 M_\odot$   $^{56}\text{Ni}$  for both cases despite the difference in the  $^{56}\text{Ni}$  distribution; thus the abundances of those isotopes produced by complete Si burning relative to  $^{56}\text{Ni}$  appear to be smaller for  $Z = 0$  ( $\sim 10^{-5} M_\odot$ ) than  $Z = 0.02$  by a factor of 2 - 4. We stress again that the  $^{44}\text{Ti}$  mass is uncertain because it significantly depends on mass cut.

$^{26}\text{Al}$  is produced in the H, He and C-burnings and the ejected mass is independent of mass cut, while its mass is smaller for smaller metallicity. For  $Z = 0.02$ , the  $^{26}\text{Al}$  mass ranges from  $1 \times 10^{-5} M_\odot$  to  $8 \times 10^{-5} M_\odot$  for the 13 to  $25 M_\odot$  stars. For  $Z = 0$ , these masses range from  $1 \times 10^{-7} M_\odot$  to  $2 \times 10^{-6} M_\odot$ .

### 6. INTEGRATED ABUNDANCES RELATIVE TO THE SOLAR ABUNDANCES

Figures 9-12 show the integrated abundances of stable isotopes in the ejecta relative to the solar values (Anders & Grevesse 1989) for the stars of  $M = 13 - 25 M_\odot$  and  $Z = 0$  and  $0.02$ . (Here we adopt the lower efficiency of mixing,  $f_k = 0.05$ .) Each yield is normalized to the solar  $^{16}\text{O}$  value.

Figure 9 shows the yields from the solar metallicity stars. The explosion energy, i.e., the final kinetic energy, is assumed to be  $E = 10^{51}$  erg and the mass cut is chosen to eject  $0.07 M_\odot$   $^{56}\text{Ni}$ . The abundance ratios are mostly consistent with the solar ratios from C to Ca, but show significant deviations from the solar ratios for heavier species. Further parameter study is necessary to see how the results depend on the metallicity,  $f_k$ , and the mass cut. The upper panel of Figure 13 shows that our result for  $f_k = 0.05$  is roughly consistent with WW95, though our  $^{12}\text{C}(\alpha, \gamma)^{16}\text{O}$  rate is smaller than WW95 by a factor of 1.2.

The results for the metal-free models are shown in Figure 10. A distinctive feature of the  $Z = 0$  models compared with the  $Z = 0.02$  models is that, alpha nuclei (from C to Zn) are much more abundant than others. In Figure 11 we show the yield ratios between  $Z = 0$  and  $Z = 0.02$ . The most evident signature of the Pop III abundance pattern appears in the large isotopic ratios for the even  $Z$  elements (such as  $^{13}\text{C}/^{12}\text{C}$ ) and the deficiency of the odd  $Z$  elements such as  $^{23}\text{Na}$ ,  $^{27}\text{Al}$ , and  $^{31}\text{P}$ . We will come back to this point in Section 8. Comparison of our results with WW95 in the lower panel of Figure 13 shows that our model has smaller abundances of the even  $Z$  neutron-rich isotopes; this is probably because WW95 included neutrino irradiation effects which we do not.

Isotopes heavier than Si are mostly produced during explosive nucleosynthesis. The explosive nucleosynthesis depends on several parameters such as the explosion energy and mass cuts which are not well determined because of the uncertainty in the explosion mechanism. Some of the parameter dependences for  $Z = 0$  are shown in Figure 12.

The difference in the bottom panel of Figure 10 and the top panel of Figure 12 is the mass cut. In the latter, deeper mass cut is chosen so that  $[^{16}\text{O}/^{56}\text{Ni}] = 0$ ; then interestingly the abundance ratios for the even  $Z$  elements up to Zn can be roughly solar. Elements heavier than Zn might also be produced in the same way though we have not calculated.

The top, 2nd and 3rd panels of Figure 12 show the dependence on the explosion energy. The influence of the higher explosion energy is mainly to shift the distribution of the peak temperature outward. As a result, the location of the mass cut affects drastically the produced amount of  $^{56}\text{Ni}$ . These figures show that Si and Ca are more abundant for a larger explosion energy.

Finally the effect of more efficient convective mixing is shown in the 2nd panel of Figure 12. It appears that this parameter choice ( $f_k = 0.15$ ) is better to reproduce the solar abundance ratio for the even  $Z$  elements. However, we need further calculations for other masses and parameters in order to find general trends.

## 7. CR, MN, CO, AND ZN

As mentioned in §1, recent high resolution abundance surveys discovered interesting trends of  $[\text{Cr}/\text{Fe}]$ ,  $[\text{Mn}/\text{Fe}]$  and  $[\text{Co}/\text{Fe}]$  with  $[\text{Fe}/\text{H}]$ , that is, both  $[\text{Cr}/\text{Fe}]$  and  $[\text{Mn}/\text{Fe}]$  decreases as metallicity declines for  $[\text{Fe}/\text{H}] = -2.4$  to  $-4.0$  while  $[\text{Co}/\text{Fe}]$  increases (McWilliam et al. 1995ab; Ryan et al. 1996; McWilliam 1997). One might suspect that these trends would be a signature of Pop III.

These trends could be explained with SNe II, if these abundance ratios strongly depend on metallicity. Figure 8 shows that the amount of iron peak elements produced by the explosive synthesis such as Cr, Mn, Co do not much depend on the initial stellar metallicity (even though Mn and Co have odd  $Z$ ). Although  $Y_e$  for  $Z = 0$  and 0.02 models is slightly different, these results show that the effect is not very large.

Therefore, other factors would be responsible to cause the above trends. In order to investigate the ratios  $[\text{Cr}/\text{Fe}]$ ,  $[\text{Mn}/\text{Fe}]$  and  $[\text{Co}/\text{Fe}]$  we look into the regions where these elements are produced. First of all,  $^{56}\text{Ni}$ , which decays into the most abundant Fe isotope  $^{56}\text{Fe}$ , is produced not only in the complete Si-burning region but also in the incomplete Si-burning region.  $^{59}\text{Cu}$ , which decays into  $^{59}\text{Co}$ , is produced in the complete Si-burning region.

$^{52}\text{Fe}$  and  $^{55}\text{Co}$ , which decay into  $^{52}\text{Cr}$  and  $^{55}\text{Mn}$ , respectively, are mostly synthesized in the incomplete Si-burning region.  $^{52}\text{Fe}$  is also synthesized in the complete Si-burning region, but not a large amount. Note that  $^{55}\text{Mn}$  and  $^{59}\text{Co}$  are the only stable isotopes of these elements and therefore, their abundances are identical with the Mn and Co element abundances.

The above discussion suggests that the choice of the mass cut can affect the ratios  $[\text{Cr}/\text{Fe}]$ ,  $[\text{Mn}/\text{Fe}]$ , and  $[\text{Co}/\text{Fe}]$ . For a deeper mass cut, the ejected mass of the complete Si-burning region is larger (i.e., the masses of Fe and Co are larger), while the ejected mass of the incomplete Si-burning region remains the same (i.e., the masses of Cr, Mn, and Fe are the same). Accordingly the ratios of  $[\text{Cr}/\text{Fe}]$  and  $[\text{Mn}/\text{Fe}]$  are smaller and  $[\text{Co}/\text{Fe}]$  is larger. For a mass cut at larger radii, these ratios show the opposite tendency. Therefore, specific choices of mass cuts in SNe II might explain the behavior of  $[\text{Cr}/\text{Fe}]$ ,  $[\text{Mn}/\text{Fe}]$ , and  $[\text{Co}/\text{Fe}]$  in the metallicity range  $-4 \leq [\text{Fe}/\text{H}] \leq -2.5$  (Nakamura et al. 1999).

The dependence of the abundance ratios on the mass cut is seen from the comparison between Figures 10 and 12. The relative thickness between the complete and the incomplete Si burning layers may also depend on the efficiency of convective mixing  $f_k$ .

Note also that Zn is produced from complete Si burning as seen in Figures 8. In order to reproduce  $[\text{Zn}/\text{Fe}] \sim 0$  as observed in metal-poor stars, the ejection of relatively large amount of complete Si burning material is necessary as seen in Figure 12 and discussed in §6. This would occur if the mass cut is as deep as discussed above (Nakamura et al. 1999) or if such complete Si burning material is preferentially ejected in a form of a jet or bullets (Umeda 1999) from the deepest layer.

## 8. POP III CHARACTERS IN THE ABUNDANCE PATTERN

Massive Pop III stars no longer exist in the present universe. However, if Pop III supernovae induced the for-

mation of low-mass stars, such stars should still alive and may be observable. Indeed some of the observed metal-poor halo stars may be such stars. If we can identify such stars, they are very useful in understanding the nucleosynthesis in the earliest universe. Also we may even be able to determine the typical mass range of Pop III stars by comparing theory with observed abundance pattern.

In the previous section we saw that the most distinctive features of the Pop III nucleosynthesis compared with Pop I and II are the abundance ratios in even  $Z$  isotopes (e.g.,  $^{12}\text{C}/^{13}\text{C}$ ) and the deficiency of the odd  $Z$  elements such as  $^{23}\text{Na}$ ,  $^{27}\text{Al}$ , and  $^{31}\text{P}$  compared with even  $Z$  elements. In this section, we discuss in more detail the metallicity dependence of the abundance pattern to find specific characteristics of Pop III abundance pattern. As described above, yields from explosive nucleosynthesis depends on the non-well-understood properties of explosion such as the mass cut, mixing, etc. Therefore, we concentrate on the elements which are not sensitive to the explosive synthesis.

## 8.1. CNO elements

In order to study the metallicity dependence of the yields in more detail, we calculate stellar evolution and explosive nucleosynthesis for the  $20 M_{\odot}$  models with  $Z = 0.02, 0.004, 0.001, 10^{-5}$  and 0. The integrated abundance ratio of some elements X to  $^{24}\text{Mg}$  relative to the solar ratio are shown in Figures 14, where  $[X/Y] \equiv \log_{10}(X/Y) - \log_{10}(X/Y)_{\odot}$ . Here  $^{24}\text{Mg}$  is used for normalization, because yield of  $^{24}\text{Mg}$  is independent of mass cut and does not significantly depend on metallicity (e.g., 0.066, 0.054, 0.040, and 0.081  $M_{\odot}$  for  $Z = 0.02, 0.004, 0.001$  and 0, respectively for the  $20 M_{\odot}$  models); furthermore observationally  $[^{24}\text{Mg}/\text{H}]$  appears to roughly correlate with metallicity  $[\text{Fe}/\text{H}]$  (Shigeeyama & Tsujimoto 1998). In these figures, the filled circles show the ratios for the  $20 M_{\odot}$  star. The asterisk, triangle, and square represent 13, 15, 25  $M_{\odot}$  models, respectively (only for  $Z=0$  and 0.02), and open circle is the  $25 M_{\odot}$   $Z = 0$  model with more efficient convective mixing ( $f_k = 0.15$ ).

These figures show that the abundance ratios for  $^{12}\text{C}$  and  $^{16}\text{O}$  are almost independent of metallicity ( $Z$ ), while the ratios for  $^{13}\text{C}$  and  $^{14}\text{N}$  are smaller for smaller metallicity.

The result for  $^{14}\text{N}$  yield is interesting. The  $[^{14}\text{N}/^{24}\text{Mg}]$  ratio decreases as metallicity gets smaller, but its metallicity dependence is sensitive to the stellar mass. For  $Z = 0$ ,  $[^{14}\text{N}/^{24}\text{Mg}]$  is larger for less massive stars and its value for the 13  $M_{\odot}$  model is only 1/4 of the solar ratio. Therefore, primordial  $^{14}\text{N}$  production from Type II supernovae may be significant. This  $^{14}\text{N}$  production mechanism by these stars are similar to the suggestion in WW95. There, they commented that in some of their unpublished early calculations the convective He-shell penetrated into the H-layer with the consequent production of large amounts of primary  $^{14}\text{N}$ . In our model also  $^{14}\text{N}$  is produced in the He-burning shell during central C-burning. In this stage, the He-shell burning becomes strong enough to form a convective layer. This convective layer reaches the H-rich layer and the CNO-cycle operates to produce  $^{14}\text{N}$ . In our model this mechanism is specific to the Pop III stars. For larger metallicity, the convective layer in the He-burning shell

is hard to reach the H-rich region without overshooting because H-shell burning is so active to form a high entropy barrier. The  $^{14}\text{N}$  production may be enhanced if we assume more efficient convective mixing as shown by the example in Figure 14 (open circle).

### 8.2. Odd $Z$ elements

The abundances of odd  $Z$  elements produced during C-burning such as  $^{23}\text{Na}$ ,  $^{27}\text{Al}$ , and  $^{31}\text{P}$  may be good indicators for the metallicity of the progenitor stars, because these elements are secondary and their abundances are expected to be smaller for smaller metallicity. Figure 14 shows that  $^{23}\text{Na}$  and  $^{27}\text{Al}$  abundances are smaller for smaller metallicity, in contrast to the primary elements such as  $^{20}\text{Ne}$  and  $^{24}\text{Mg}$ . These figures show, however, that the declines of  $^{23}\text{Na}/^{24}\text{Mg}$  and  $^{27}\text{Al}/^{24}\text{Mg}$  toward smaller metallicity almost saturate for  $Z/Z_{\odot} \lesssim 5 \times 10^{-4}$ . Hence it might be difficult to distinguish the Pop III abundance pattern from the abundance pattern of very low-metal Pop II stars only by these elements. Nevertheless we may say that the stars with the lowest  $^{23}\text{Na}/^{24}\text{Mg}$  and  $^{27}\text{Al}/^{24}\text{Mg}$  are most likely composed of the lowest metallicity SN ejecta.

Figure 15 shows the observed abundance ratios  $[\text{Na}/\text{Mg}]$  and  $[\text{Al}/\text{Mg}]$  in stars of the halo and the local disk (McWilliam et al. 1995ab; Ryan & Norris 1991; Edvardsson et al. 1993). The stars with the Pop III abundance pattern, if they exist, should belong to the low-metal stars ( $[\text{Mg}/\text{H}] \lesssim -2$ ), but not necessarily the lowest metallicity stars because of the following reason. Such stars are composed of Pop III SNe ejecta mixed with interstellar matter (ISM). The amount of ISM mixed with the SN ejecta is estimated by Ryan et al. (1996). It depends on several uncertain factors but typically the metallicity of the mixed ejecta ranges from  $[\text{Mg}/\text{H}] \sim -4$  to  $-2$  (see also Nakamura et al. 1999, Shige-yama & Tsujimoto 1998).

The observed patterns of  $[\text{Na}/\text{Mg}]$  and  $[\text{Al}/\text{Mg}]$  vs  $[\text{Mg}/\text{H}]$  are similar. For  $[\text{Mg}/\text{H}] \lesssim -2$ , the lower bounds are almost constant ( $\sim -1$ ) and upper bounds increase with  $[\text{Mg}/\text{H}]$ . The existence of the constant lower bounds is consistent with our results shown in Figures 14; it can be explained if these stars are composed of ejecta of Pop III or very low metal Pop II supernovae. Although only from these data it is hard to find the differences between the Pop III and the very low metal Pop II abundance, or the differences of progenitor masses, further theoretical and observational study may make discrimination possible.

### 8.3. Alpha Elements/ $Fe$

In §6 and Figure 12, we discuss the cases with  $^{16}\text{O}/^{56}\text{Ni} = 0$ . These SNe produce a large amount of  $^{56}\text{Ni}$  ( $\sim 0.3M_{\odot}$ ), which is comparable to hypernovae SN1998bw and SN1997ef (Iwamoto et al. 1998, 1999) and even Type Ia supernovae (Nomoto et al. 1984).

In this connection, the abundance pattern of the very metal-poor binary CS22873-139 ( $[\text{Fe}/\text{H}] = -3.4$ ) is interesting. This binary has only the upper limit to  $[\text{Sr}/\text{Fe}] < -1.5$ , thus being suggested to be a second generation star (Nordstrom et al. 1999). Although  $[\text{Al}/\text{Fe}] \sim -0.6$  is too large for Pop III, other abundance features should be examined.

Interesting pattern is that this binary shows almost the solar  $\text{Mg}/\text{Fe}$  and  $\text{Ca}/\text{Fe}$  ratios. This would not mean that Type Ia supernovae contributed to the enrichment of Fe for such a metal-poor star. We rather suggest that the abundance pattern of this binary originates from hypernovae. Another feature of CS22873-139 is enhanced  $\text{Ti}/\text{Fe}$  ( $[\text{Ti}/\text{Fe}] \sim +0.6$ ; Nordstrom et al. 1999), which also seems to be the result from hyper-energetic or hyper-asymmetric explosion.

Since Pop III stars may consist of many massive stars that undergo hypernova-like explosions,  $[\alpha \text{ element}/\text{Fe}] \sim 0$  could possibly be a signature of Pop III SNe.

## 9. SUMMARY

We calculate pre-supernova evolutions and supernova explosions of massive stars ( $M = 13 - 25M_{\odot}$ ) for various metallicities. We find some characteristic abundance patterns of nucleosynthesis in the metal-free (Pop III) stars.

The most distinctive features of the Pop III nucleosynthesis compared with Pop I and II are that, for  $Z = 0$ , alpha nuclei (from C to Zn) are much more abundant than others. (The abundance pattern of  $\alpha$ -nuclei can be similar to the solar abundance.) Therefore, by looking for the smallest isotopic ratios for the even  $Z$  elements (such as  $^{13}\text{C}/^{12}\text{C}$ ) or the smallest abundance of odd  $Z$  elements in the metal-poor star abundances, we can find candidates of the stars having Pop III abundance pattern. Also, near solar ratios of alpha elements/Fe might be a signature of Pop III which could produce a large amount of Fe in hyper-energetic explosion.

The abundance ratios of odd  $Z$  to even  $Z$  elements such as  $\text{Na}/\text{Mg}$  and  $\text{Al}/\text{Mg}$  become smaller for lower metallicity. However these ratios almost saturate below  $Z \lesssim 10^{-5}$ , and  $[\text{Na}, \text{Al}/\text{Mg}] \sim -1$  for Pop III and low metal Pop II nucleosynthesis. This result is consistent with abundance pattern of metal poor stars, in which these ratios also saturate around  $-1$ . We suggest that these stars with the lowest  $[\text{Na}/\text{Mg}]$  or  $[\text{Al}/\text{Mg}]$  may contain the abundance pattern of Pop III nucleosynthesis.

Metal poor stars show interesting trends in the ratios of  $[\text{Cr}, \text{Mn}, \text{Co}/\text{Fe}]$ . We discuss that these trends are not explained by the differences in metallicity, but by the relative thickness between the complete and the incomplete Si burning layers. Large  $[\text{Co}/\text{Fe}]$  and small  $[\text{Cr}, \text{Mn}/\text{Fe}]$  values found in the observations are explained if mass cut is deep or if matter is ejected from the complete Si burning layer in a form of a jet or bullets.

We also find that primary  $^{14}\text{N}$  production occurs in the massive Pop III stars, because these stars have radiative H-rich envelopes so that the convective layer in the He-shell burning region can reach the H-rich region. Then primary  $^{14}\text{N}$  production by NO-cycle can occur without overshooting.

Further study may make it possible to determine the metallicity and progenitor mass ranges of a SN which produced the metal-poor stars.

We would like to thank M. Hashimoto and H. Saio for providing us with the basis of the present evolutionary code. This work has been supported in part by the Grant-in-Aid for by COE Scientific research (07CE2002, 0980203)

of the Japanese Ministry of Education, Science, and Culture.

## REFERENCES

- Anders E., & Grevesse, N., 1989, *Geochim. Cosmochim. Acta* 53, 197
- Arnett, W.D. 1996, *Supernovae and Nucleosynthesis* (Princeton Univ. Press)
- Arnett, W.D., Bahcall, J.N., Kirshner, R.P., & Woosley, S.E. 1989, *Ann. Rev. Astron. Ap.*, 27, 629
- Audouze, J., & Silk, J. 1995, *ApJ*, 451, L49
- Barkat, Z., & Marom, A. 1990, in *Supernovae*, ed. J.C. Wheeler et al. (World Scientific), 95
- Caughlan, G.R., & Fowler, W.A., 1988, *Atomic Data & Nucl. Data Tables*, 40, 283 (CF88)
- Castellani, V., Chieffi, A., & Tornambé 1983, *ApJ*, 272, 249
- de Jager, C., Nieuwenhuijzen, H., & van der Hucht, K.A. 1988, *A&AS*, 72, 259
- Edvardsson, B., Andersen, J., Gustafsson, b., Lamgert, D. L., Nissen, P. E., & Tomkin, J. 1993, *A&Ap*, 275, 101
- Fowler, W.A. 1984, *Rev. Mod. Phys.*, 56, 149
- Galama, T.J. et al. 1998, *Nature*, 395, 670
- Germany, L. et al. 1999, *ApJ*, submitted (astro-ph/9906096)
- Hashimoto, M. 1995, *Prog. Theor. Phys.*, 68, 795
- Hashimoto, M., Nomoto K., & Shigeyama, T., 1989, *A&A*, 210, L5
- Hix, W.R. & Thielemann, F.-K. 1996, *ApJ*, 460, 869
- Iglesias, C.A., & Rogers, F.F., 1993, *ApJ*, 412, 752
- Iwamoto, K., Mazzali, P.A., Nomoto, K., Umeda, H., Nakamura, T., et al. 1998, *Nature*, 395, 672
- Iwamoto, K., Nakamura, T., Nomoto, K., Mazzali, P.A., Danziger, J., et al. 1999, *ApJ*, submitted (astro-ph/9807060)
- Kudritzki, R.P., Pauldrach, A., Puls, J., & Abbott, D.C. 1989, 219, 205
- Kumagai, S., Shigeyama, T., Nomoto K., et al. 1989 *ApJ*, 345, 412
- Kumagai, S., Shigeyama, T., Nomoto K., Hashimoto, M., & Itoh, M. 1993, *A&A*, 273, 153
- Limongi, M., Chieffi, A., & Straniero, O. 1998, in *Nuclei in the Cosmos V*, eds. N. Prantzos, S. Harissopulos (Editions Frontieres), 144; private communication (LCS)
- McWilliam, A., Preston, G.W., Sneden, C., & Sheckman, S. 1995a, *AJ*, 109, 2736
- McWilliam, A., Preston, G.W., Sneden, C., & Searle, L. 1995b, *AJ*, 109, 2757
- McWilliam, A. 1997, *ARA&A*, 35, 503
- Nakamura, T., Umeda, H., Nomoto, K., Thielemann, F.-K., & Burrows, A. 1999, *ApJ*, 517, 193
- Nomoto, K., & Hashimoto, M. 1988, *Phys. Rep.*, 163, 13 (NH88)
- Nomoto, K., Iwamoto, K., Tsujimoto, T., & Hashimoto, M. 1993, in *Frontiers of Neutrino Astrophysics*, ed. Y. Suzuki and K. Nakamura (Tokyo: Universal Academy Press), 235
- Nomoto, K., Shigeyama, T., Kumagai, S., Yamaoka, H., & Suzuki, T. 1994, in *Supernovae (Les Houche Session LIV)*, eds. S. Bludman et al. (Elsevier Science), 489
- Nomoto, K., Thielemann, F.-K., & Yokoi, K. 1984, *ApJ*, 286, 644
- Nomoto, K., et al. 1997, *Nuclear Phys. A*616, 79
- Nordstrom, B. et al. 1999, in this volume
- Rayet, M., Arnould, M., Hashimoto, M., Prantzos, N., & Nomoto, K. 1995, *A&A*, 298, 517
- Ryan, S.G., & Norris, J.E. 1991, *AJ*, 101, 1835
- Ryan, S.G., Norris, J.E., & Beers, T.C. 1996, *ApJ*, 471, 254
- Saio, H., & Nomoto, K., 2000, in *Computational Astrophysics: Stellar Physics*, eds. Kudritzki, R., Mihalas, D., Nomoto, K., & Thielemann, F.-K. (New York: Springer), in press
- Shigeyama, T. & Tsujimoto, T. 1998, *ApJ*, 507, L135
- Spruit, H.C. 1992, *A&A*, 253, 131
- Thielemann, F.-K., Nomoto, K., & Hashimoto, M. 1994, in *Les Houches, Session LIV* ed. J. Audouze, S. Bludman, R. Mochkovitch & J. Zinn-Justin, 629
- Thielemann, F.-K., Nomoto, K., & Hashimoto, M. 1996, *ApJ*, 460, 408
- Tsujimoto, T., Nomoto, K., Yoshii, Y., Hashimoto, M., S. Yanagida, & Thielemann, F.-K. 1995, *MNRAS* 277, 945
- Turatto, M., Suzuki, T., et al. 1999, *ApJ*, submitted (astro-ph/9910324)
- Umeda, H. 1999, *ApJ*, in press (astro-ph/9911135)
- Umeda, H., Nomoto, K., Yamaoka, H., & Wanajo, S. 1999, *ApJ*, 513, 861
- Woosley, S.E., Arnett, W.D., & Clayton, D.D., 1973, *ApJ*, Suppl. 26, 231
- Woosley, S. E., Eastman, R. G., & Schmidt, B.P. 1999, *ApJ*, 516, 788
- Woosley, S.E., & Weaver, T., 1995, *ApJS*, 101, 181 (WW95)

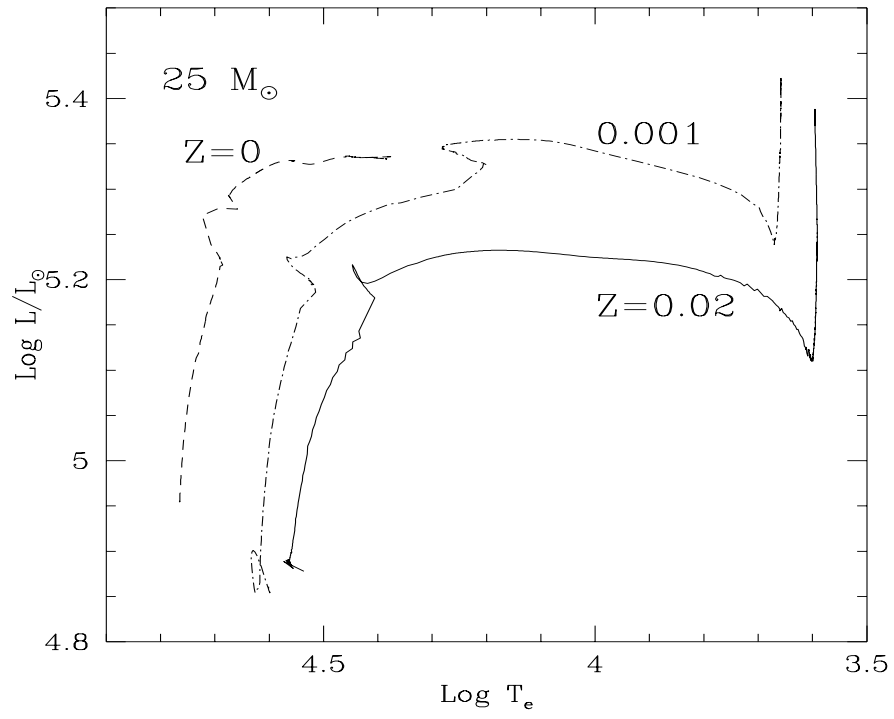


FIG. 1.— The H-R diagram of the  $25 M_{\odot}$  stars with various metallicities.

## Evolution and Nucleosynthesis of Metal-Free Massive Stars

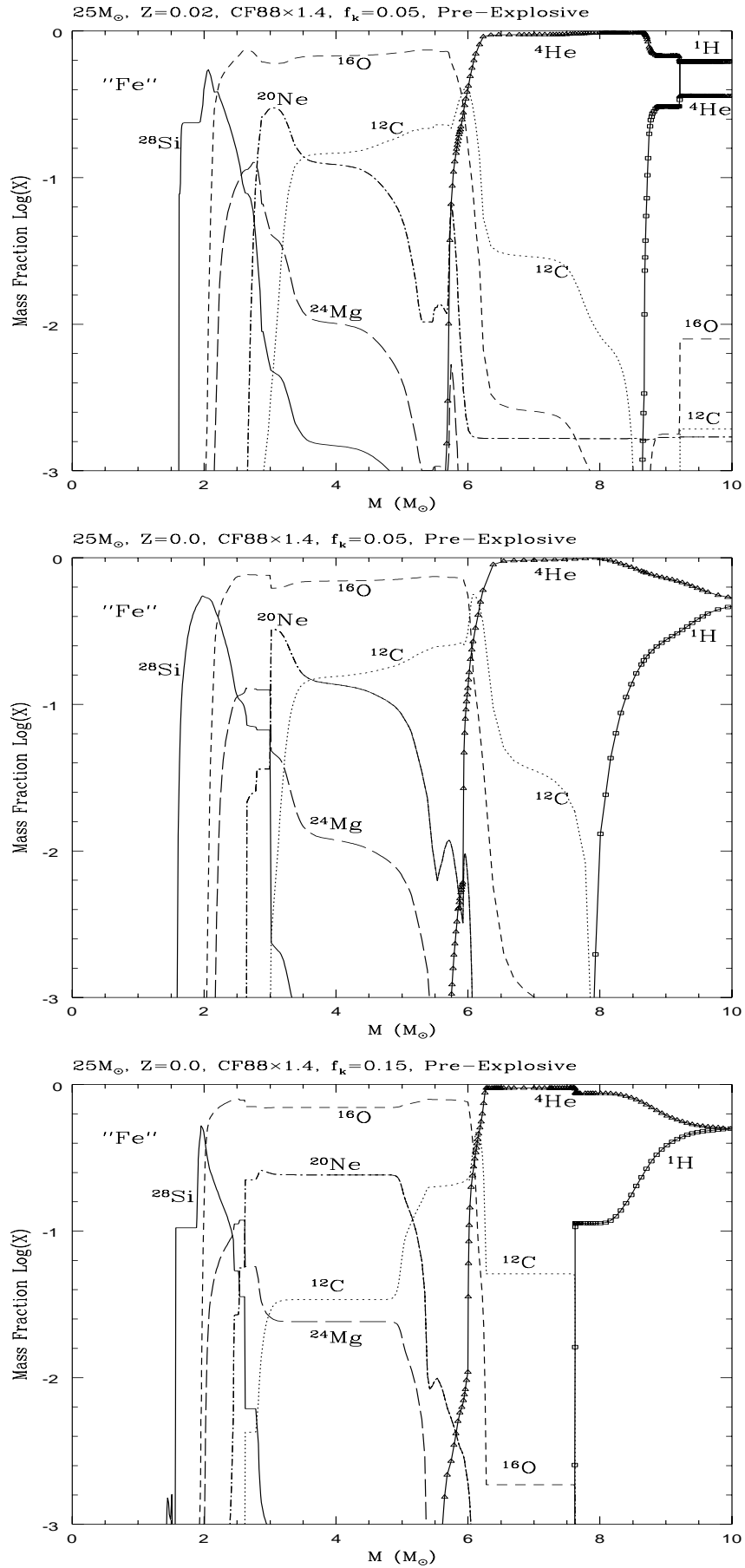


FIG. 2.— Presupernova abundance distribution. The top and the middle panels show the cases with  $Z = 0.02$  and  $Z = 0$ , respectively. The bottom one is the  $Z = 0$  case with a more efficient convective mixing ( $f_k = 0.15$ ) than others.



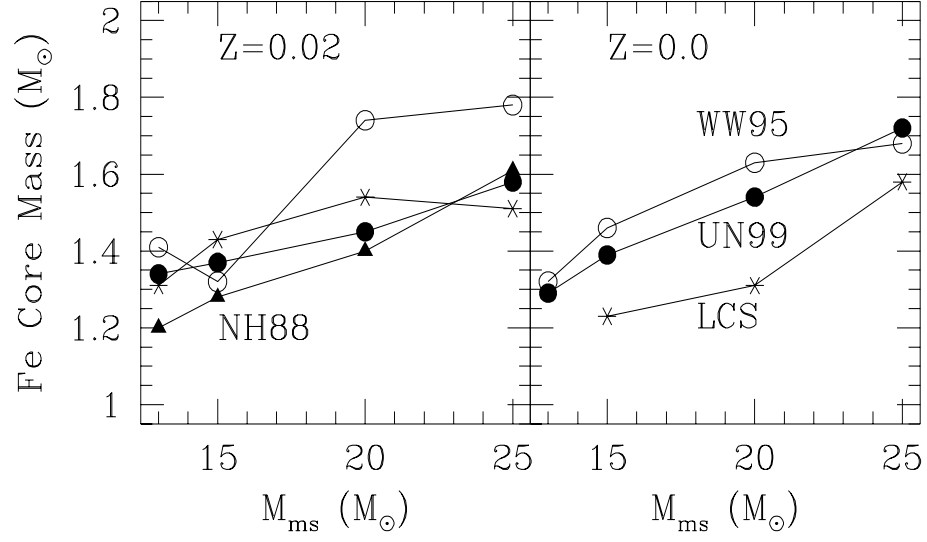


FIG. 3.— The Fe core mass as compared with other works.

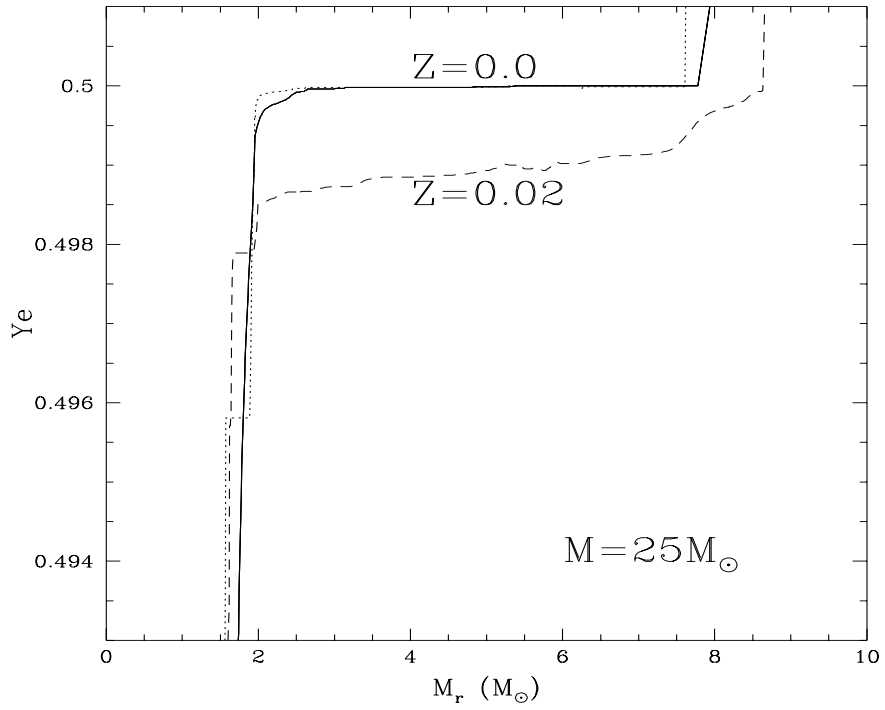


FIG. 4.—  $Y_e$  distribution of the pre-explosive  $25 M_{\odot}$  stars for  $Z = 0$  and  $0.02$ . The solid and dotted lines corresponds to  $f_k = 0.05$  and  $0.15$  models, respectively.

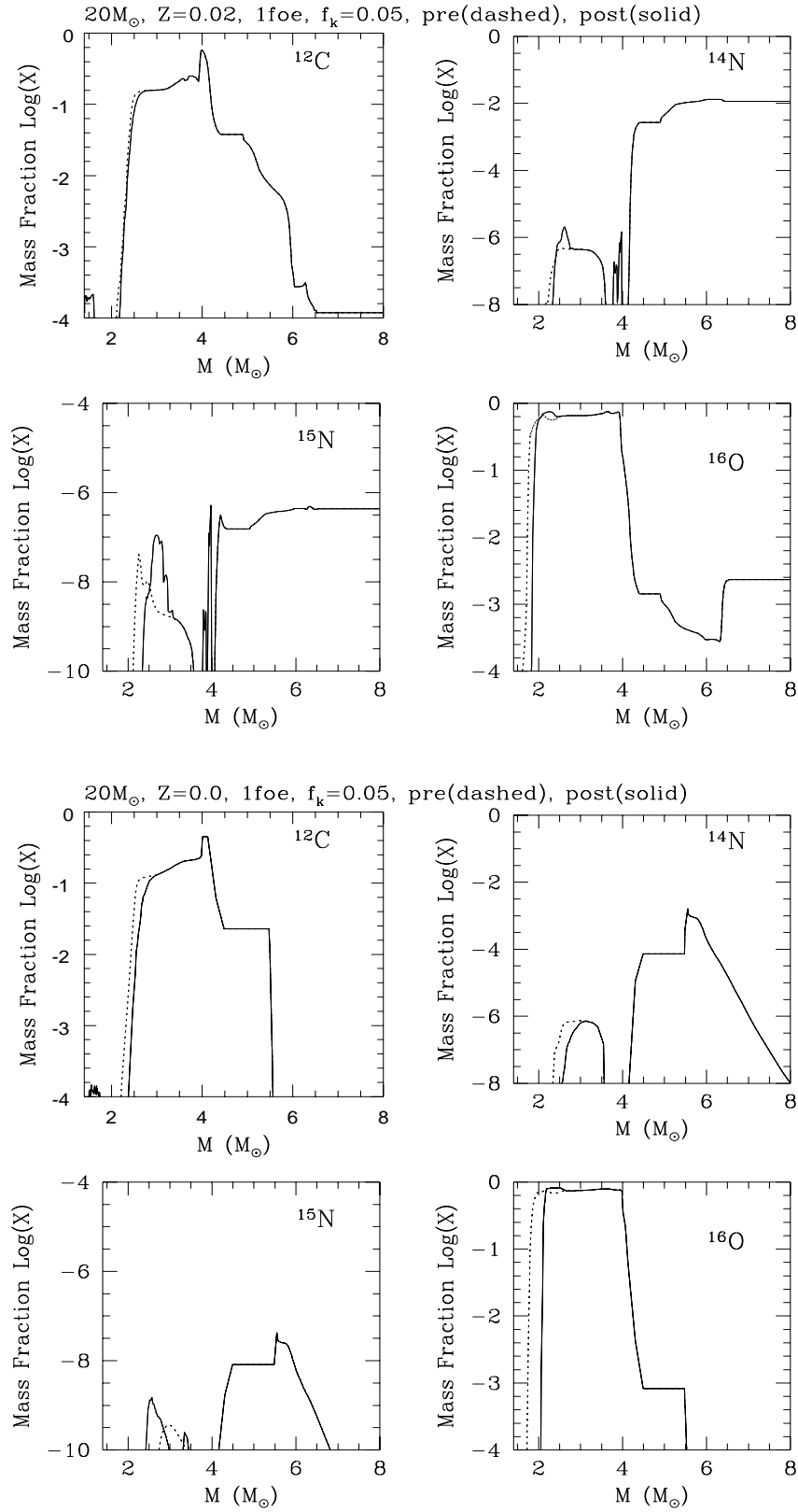


FIG. 5.— Pre and post-explosive abundance distribution of  $^{12}\text{C}$ ,  $^{14}\text{N}$ ,  $^{15}\text{N}$ ,  $^{16}\text{O}$  for  $20M_{\odot}$ ,  $Z=0.02$  (upper 4 panels) and  $Z=0$  (lower 4 panels) models.



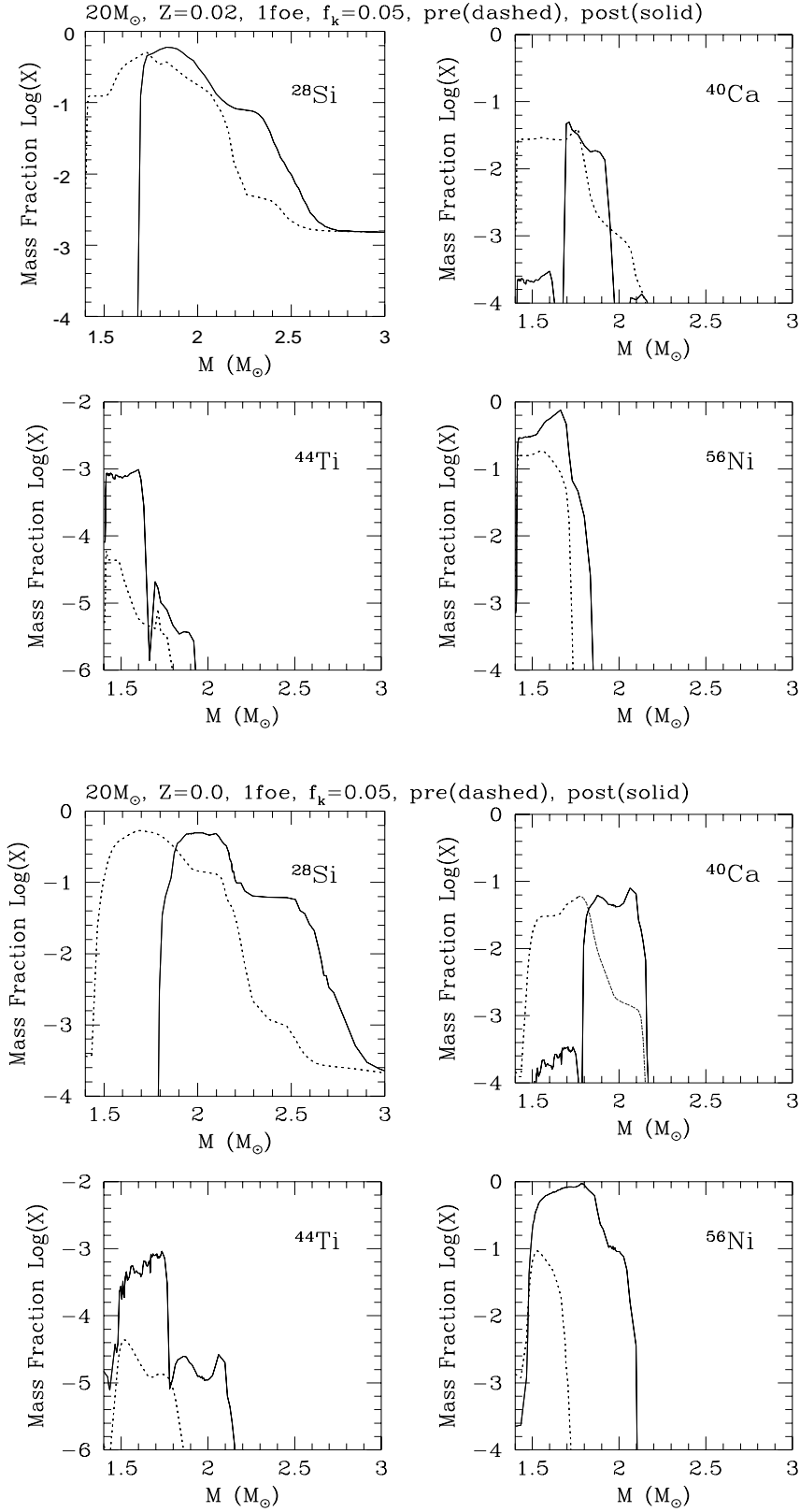


FIG. 7.— Pre and post-explosive abundance distribution of  $^{28}\text{Si}$ ,  $^{40}\text{Ca}$ ,  $^{44}\text{Ti}$ ,  $^{56}\text{Ni}$  for the 20  $M_{\odot}$ ,  $Z = 0.02$  (upper 4 panels) and  $Z = 0$  (lower 4 panels) models.

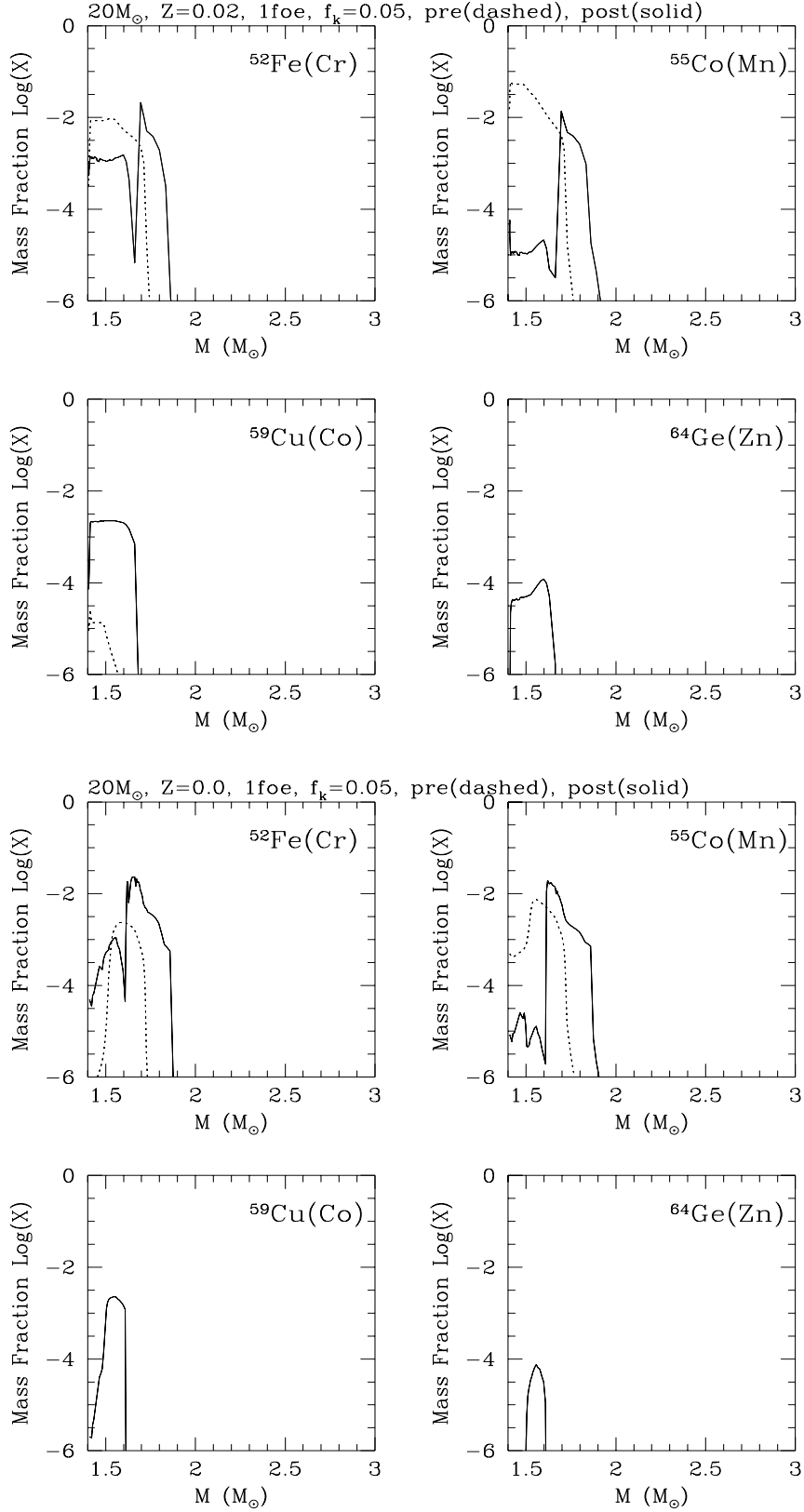


FIG. 8.— Pre and post-explosive abundance distribution of  $^{52}\text{Fe}$ ,  $^{55}\text{Co}$ ,  $^{59}\text{Cu}$ ,  $^{64}\text{Ge}$  for the 20  $M_{\odot}$ ,  $Z = 0.02$  (upper 4 panels) and  $Z = 0$  (lower 4 panels) models. These unstable isotopes are main sources to decay into Cr, Mn, Co and Zn, respectively.

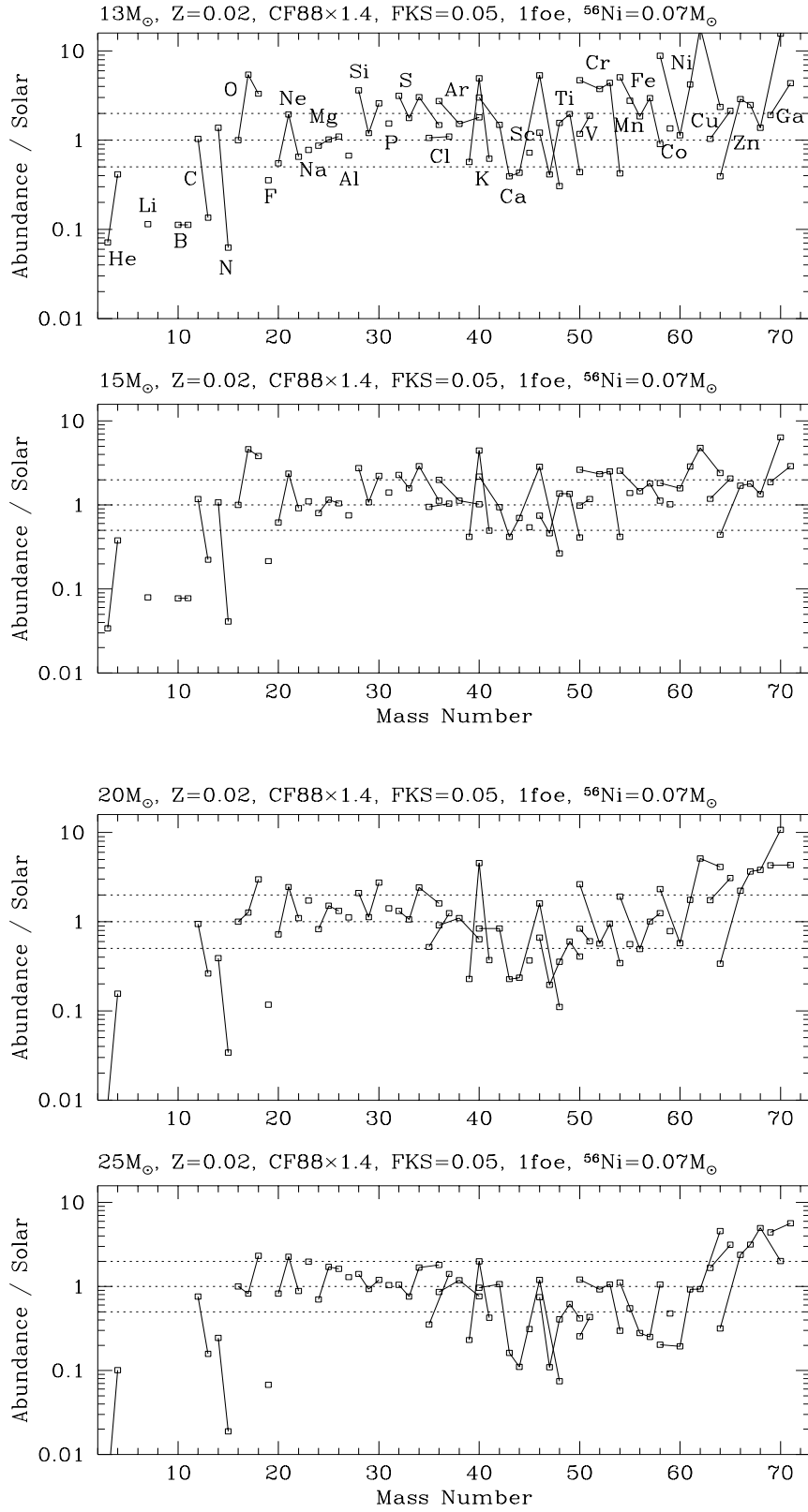


FIG. 9.— Abundances for  $Z = 0.02$ ,  $M = 13 - 25 M_{\odot}$  models normalized by the solar abundances.

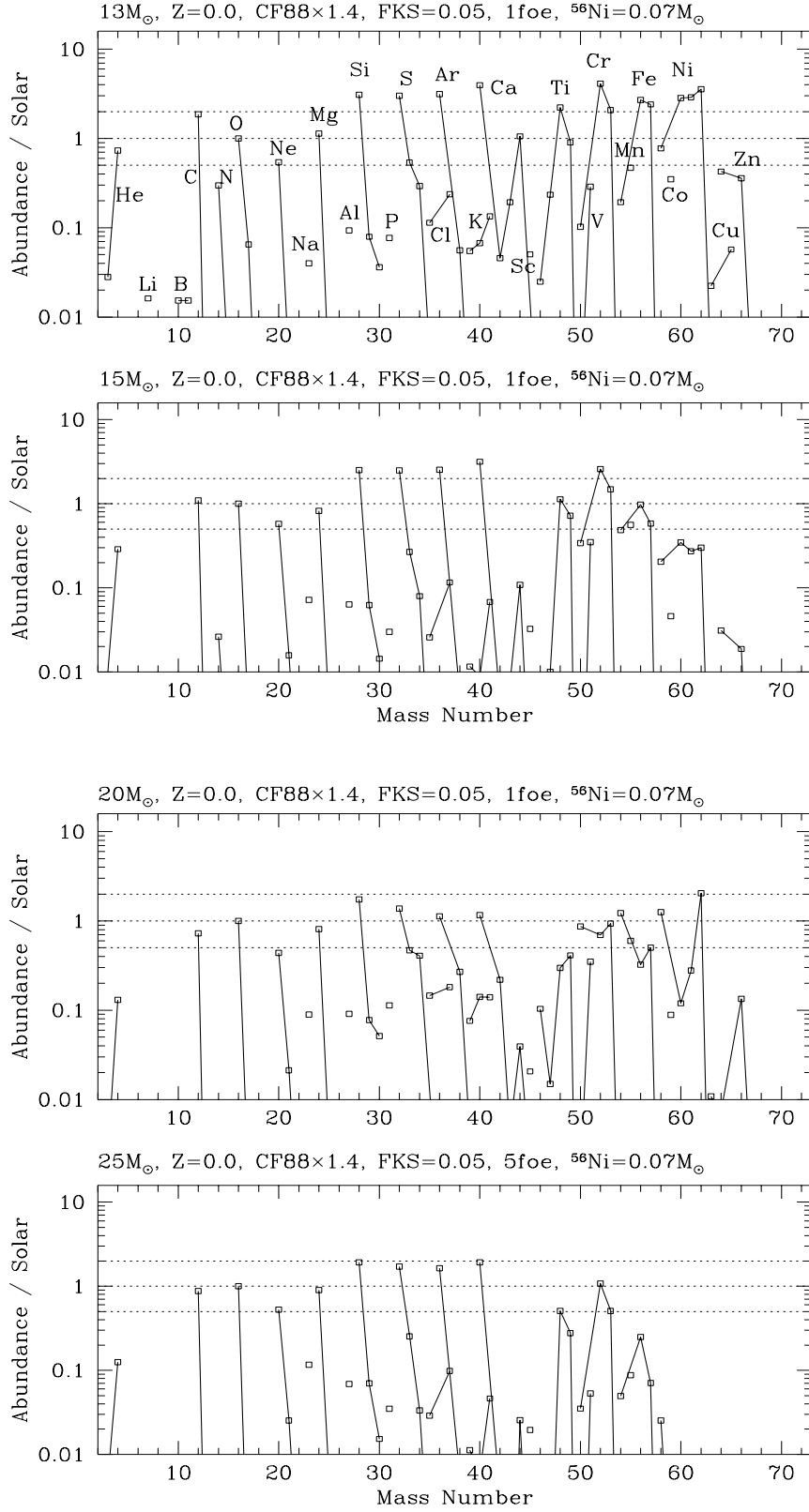


FIG. 10.— Abundances for  $Z = 0$ ,  $M = 13 - 25 M_{\odot}$  models normalized by the solar abundances.

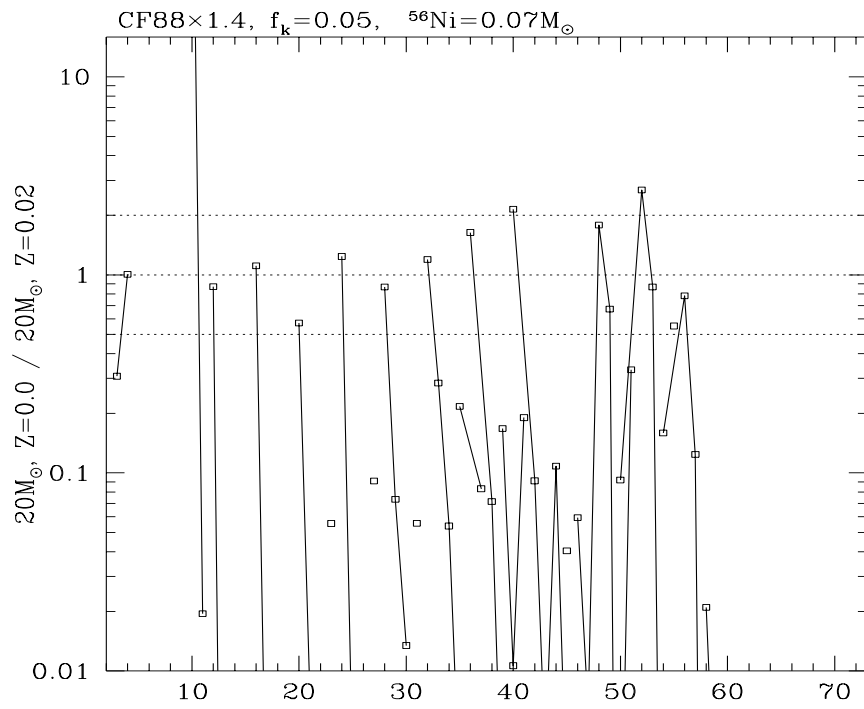


FIG. 11.— Comparison of the  $20 M_\odot$  star yields between  $Z = 0$  and  $0.02$ .



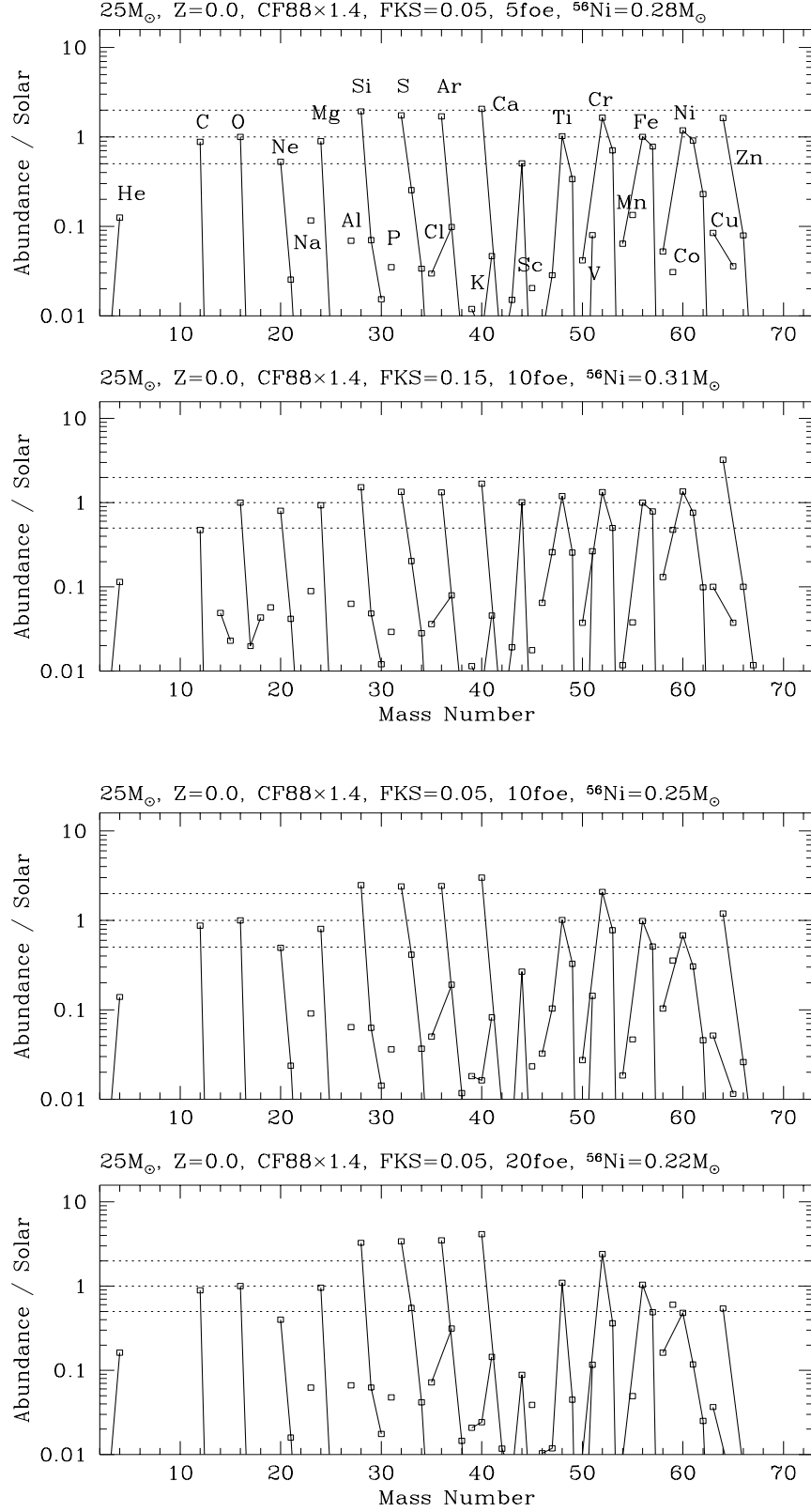


FIG. 12.— Parameter dependence of the 25  $M_{\odot}$ ,  $Z = 0$  model yields. From top to the bottom, explosion energy is varied as 5, 10, 10 and 20 foe ( $= 10^{51}$  erg). Mass cut is chosen for  $[^{16}O/^{56}Ni] = 0$ . The differences of the 2nd and 3rd panels are in the choice of convective mixing parameter  $f_k$ . Second one is a case for more efficient mixing.

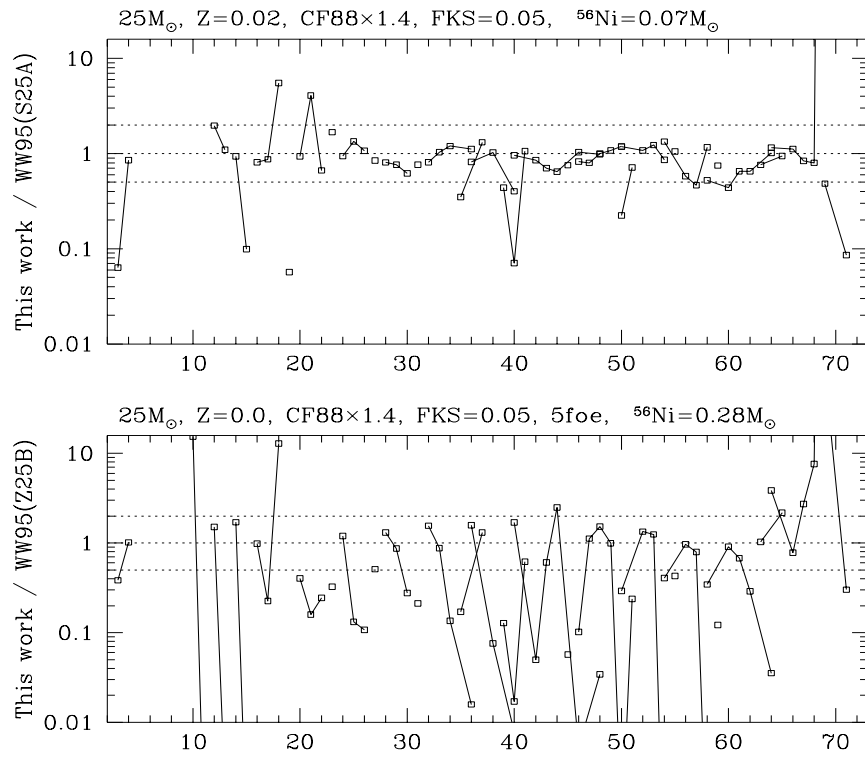


FIG. 13.— Comparison of this work with Woosley & Weaver (1995).

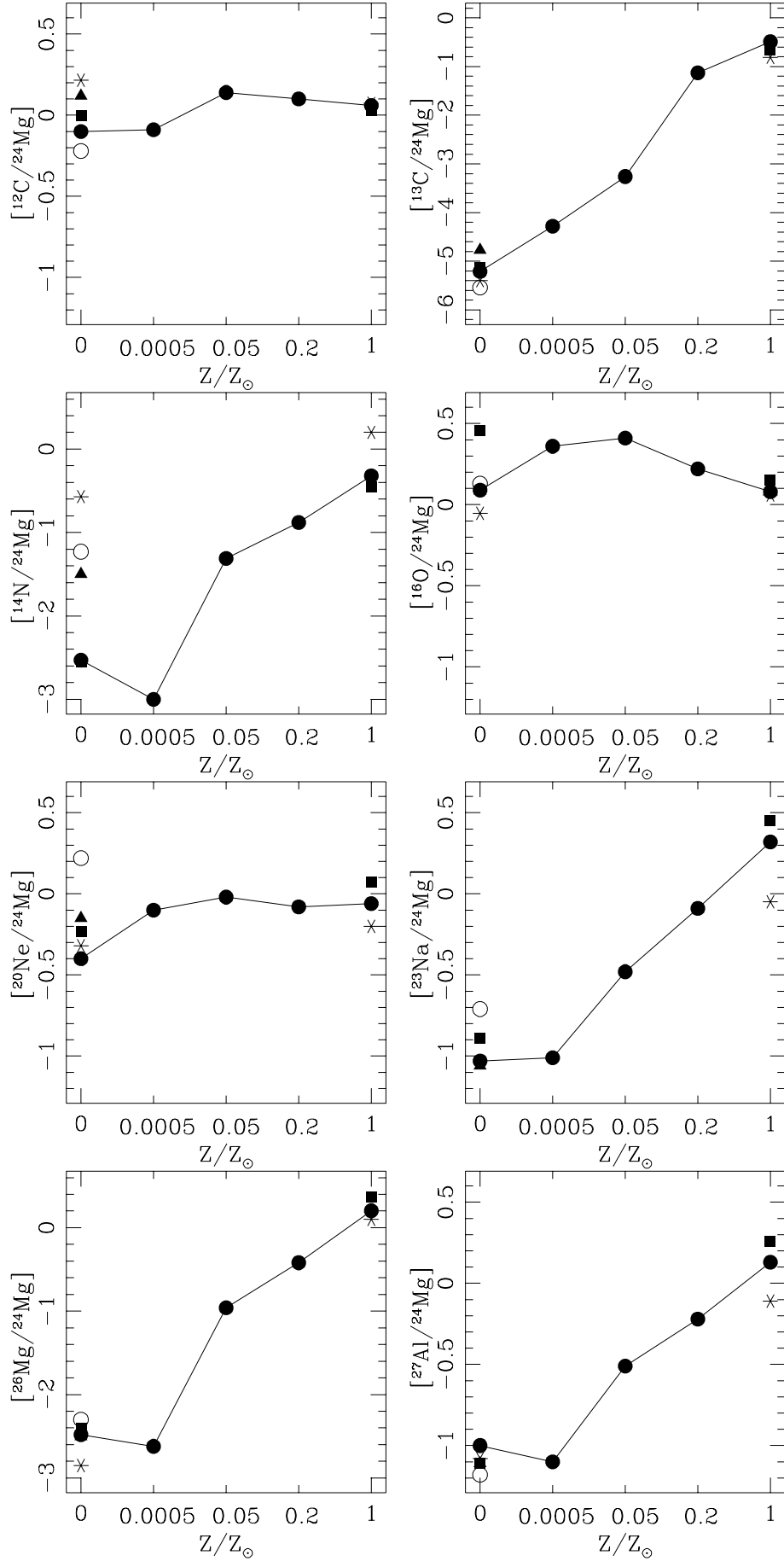


FIG. 14.— Metallicity dependence of the integrated abundance ratio of elements X to  $^{24}\text{Mg}$  relative to the solar ratio.

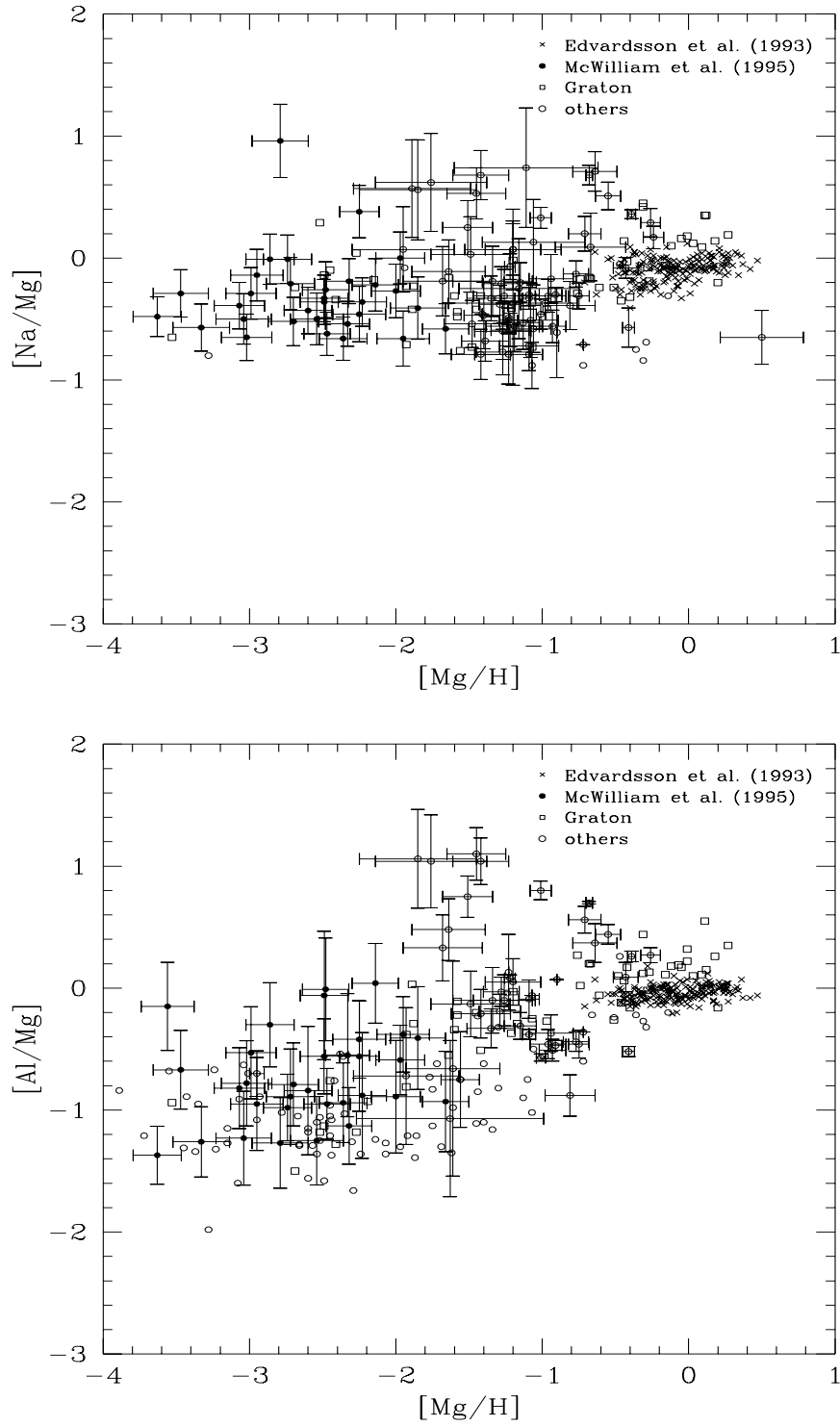


FIG. 15.— Observed abundance ratios  $[Na/Mg]$  and  $[Al/Mg]$  in stars of the halo and the local disk.